Heavy-Fermion Valence-Bond Liquids in Ultracold Atoms: Cooperation of the Kondo Effect and Geometric Frustration

L. Isaev and A. M. Rey

Phys. Rev. Lett. **115**, 165302 — Published 16 October 2015

DOI: 10.1103/PhysRevLett.115.165302

Heavy-fermion valence-bond liquids in ultracold atoms: Cooperation of Kondo effect and geometric frustration

L. Isaev and A. M. Rey
JILA, NIST & Department of Physics, University of Colorado, 440 UCB, Boulder, CO 80309, USA

We analyze a microscopic mechanism behind coexistence of a heavy Fermi liquid and geometric frustration in Kondo lattices. We consider a geometrically frustrated periodic Anderson model and demonstrate how orbital fluctuations lead to a Kondo-screened phase in the limit of extreme strong frustration when only local *singlet* states participate in the low-energy physics. We also propose a setup to realize and study this exotic state with $SU(3)$-symmetric alkaline-earth cold atoms.

PACS numbers: 71.27.+a, 75.10.Kt, 67.85.-d, 37.10.Jk

Introduction. Geometric lattice frustration plays a crucial role in Mott insulators [1] where it usually suppresses long-range magnetism by enhancing the number of competing magnetic ground states. At zero temperature, this degeneracy may be relieved in favor of a quantum non-magnetic phase such as a spin liquid or valence bond ordering [2]. On the contrary, lattice topology in most metals is less important due to long-range magnetic interactions mediated by the itinerant electrons and small static magnetic moments.

The situation is different in cases when magnetic and itinerant behaviors originate from physically distinct degrees of freedom [3]. For example, in heavy-fermion (HF) metals [4, 5] magnetic moments arise from localized $4f$ or $5f$-electrons, while conduction electrons typically reside in extended atomic s-orbitals. Low-temperature properties of such systems are driven by several opposing quantum many-body effects: (i) Kondo screening, i.e. formation of singlets between local moments and itinerant electrons that gives rise to "heavy" quasiparticle states with delocalized f-electrons; (ii) local-moment long-range magnetism; and (iii) non-magnetic states due to lattice frustration that involve singlets only among local spins. Geometrically frustrated f-electron compounds [or Kondo lattices (KLs)] such as Yb_2Pt_2Pb [6] received much attention in the recent years [7–10].

The magnetism, Kondo effect, and geometric frustration compete because they involve same local electrons which can not simultaneously form singlets with each other and the conduction band. This observation underpins the generic phase diagram of HF materials [7] that classifies them according to the amount of quantum fluctuations of local magnetism [11], and precludes Kondo screening in strongly-frustrated lattices. The antagonism between Kondo effect and lattice frustration only occurs in cases that involve pure spin degrees of freedom. In contrast, in systems with multiple local orbitals, orbital fluctuations allow local *spin singlets* to participate in the Kondo screening [12, 13] together with the usual "spinful" states. If the singlets were due to frustration, the local orbital fluctuations might provide a pathway towards a strongly-frustrated Kondo-screened state.

In the present Letter we argue that such phase with coexisting Kondo and frustration-driven local-spin singlets can indeed be realized. To demonstrate this, we consider a toy system – a periodic Anderson model on a triangular tube lattice (TTL) of Fig. 1(a) with frustrated triangular plaquettes (due to large antiferromagnetic exchange interaction between localized electrons) in the Kondo regime when valence fluctuations are suppressed and each plaquette has a spin-singlet ground state (GS) with exactly two fermions. Because of different possible arrangements of local *valence bond* (VB) singlets [14], this GS is *triply degenerate*. Although local spins are quenched in the singlet states, orbital fluctuations [Fig. 1(b)] allow mixing of the VB configurations by the Anderson hybridization with the conduction band, and give rise to a robust Kondo-screened GS with heavy quasiparticles and delocalized VB singlets [Fig. 1(c)].

This KL can be implemented using fermionic alkaline-earth atoms (AEAs), i.e. atoms with two outer electrons, in an optical lattice [see Fig. 1(d)]. AEAs prepared in the two lowest clock states ($^1S_0$ and $^3P_0$) with total angular momentum $J = 0$ show a strict decoupling of electronic orbital and nuclear-spin degrees of freedom, and obey an accurate $SU(N \leqslant 2I + 1)$ (I is the nuclear spin) symmetry in the two-body collisions [15] which has been recently verified with ^{87}Sr [16] and ^{173}Yb [17, 18]. Our key observation is that the local VB singlets can be encoded with entangled states of two AEAs [Fig. 1(e)] prepared in different clock configurations and three nuclear spin levels. The degeneracy of these states is *guaranteed by the* $SU(N = 3)$ *symmetry*. The entangled atomic pairs are loaded in the lowest, strongly localized, band of a *magic* optical lattice whose trapping potential does not affect clock transitions [19], and *implement the locally frustrated plaquettes* (the optical lattice itself does not need to be geometrically frustrated). The conduction electrons are simulated by placing AEAs in a higher, itinerant band.

At low energies, both of the above systems are described by a KL model with a peculiar $SU(3)$ structure. In the metallic regime, its GS is a Fermi [in one dimension (1D), Luttinger] liquid consisting of delocalized VB singlets (AEA pairs) screened by itinerant fermions, that

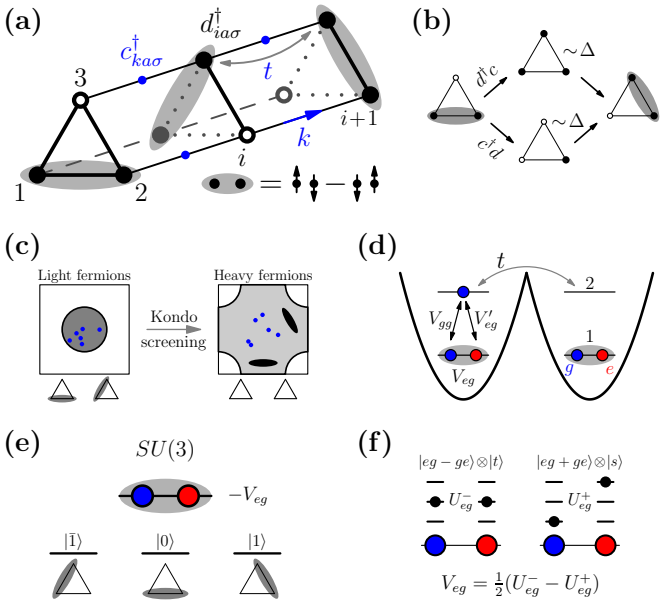

FIG. 1. Panel (a) The triangular tube lattice. Black and blue circles denote local ($d^\dagger_{ia\sigma}$) and itinerant ($c^\dagger_{ka\sigma}$) electrons. Grey ellipses are VB singlets (2) (empty circles indicate holes). Itinerant fermions propagate (by hopping between triangles with an amplitude t) in the leads with momentum k. (b) Valence fluctuations away from the two-electron singlet GS of a triangle, leading to VB flips. (c) Schematic plot of the VB delocalization and heavy-fermion formation due to Kondo screening. Shaded regions are Fermi surfaces in the Brillouin zone. (d) Magic optical lattice that implements the frustrated KL model (3) [band 1 (2) is localized (itinerant)]. Red and blue circles are AEAs in $^3P_0$ (e) and $^1S_0$ (g) clock states. Grey ellipses show local e-g entangled states (with energy $-V_{eg}$). V'_{eg} and V_{gg} are the inter-band exchange interactions ($V_{eg} \gg V'_{eg}, |V_{gg}|$). (e) Mapping from VB singlets on a triangle to lowest-energy e-g pair states for $SU(3)$ AEAs. (f) Two different scattering lengths for spin symmetric $|t\rangle$ and anti-symmetric $|s\rangle$ channels. The three levels indicate nuclear spin states for each atom (black circle marks a populated state).

can be viewed as a short-range resonant VB spin liquid [20] *stabilized by the Kondo effect*.

Toy model: $SU(3)$ KL on a TTL. Let us consider a periodic Anderson model on the lattice of Fig. 1(a):

$$H^{TTL} = \sum_{ka\sigma} \varepsilon_{k\sigma} c^\dagger_{ka\sigma} c_{ka\sigma} + v \sum_{ia\sigma} (c^\dagger_{ia\sigma} d_{ia\sigma} + \text{h.c}) + \quad (1)$$
$$+ \sum_i \left[J_H \boldsymbol{S}^2_d(x_i) - \epsilon_d N_d(x_i) + U \sum_{a\neq b} n^d_{ia} n^d_{ib} \right] + H_{\rm mix},$$

which describes a system of conduction electrons $c_{ka\sigma}$ with momentum k in the ath lead ($a = 1 \ldots 3$), spin $\sigma = \{\uparrow, \downarrow\}$, hybridized (via an amplitude v) with local electrons $d_{ia\sigma}$ at each vertex a of a triangle at position $x_i = i$. $N_d = \sum_a n^d_{ia} = \sum_{a\sigma} d^\dagger_{ia\sigma} d_{ia\sigma}$ and $\boldsymbol{S}_d = \frac{1}{2} \sum_{a\alpha\beta} d^\dagger_{ia\alpha} \boldsymbol{\sigma}_{\alpha\beta} d_{ia\beta}$ ($\boldsymbol{\sigma}$ are Pauli matrices) define electron number and total spin of a triangle. The dispersion $\varepsilon_{k\sigma} = \epsilon_k - h\sigma$ includes a small (compared to other magnetic interactions) Zeeman splitting h whose role we explain later. The term $H_{\rm mix}$ describes mixing of fermions in different leads a and for now will be ignored.

There are several energy scales associated with each triangle: local binding energy $\epsilon_d > 0$, the nearest-neighbor (NN) Coulomb repulsion U, "Hund" energy $J_H \geqslant 0$ that forces the lowest total spin S_d, and an infinitely large on-site Coulomb repulsion preventing double occupancy of any vertex a. We focus on a two-electron $S_d = 0$ subspace which contains a three-fold degenerate GS when $U - \frac{3}{4} J_H < \epsilon_d < 2U + \frac{3}{4} J_H$:

$$|a\rangle_i = \tfrac{1}{\sqrt{2}} \sum\nolimits_{b'b} s^a_{b'b} d^\dagger_{ib'\uparrow} d^\dagger_{ib\downarrow} |\text{vac}\rangle, \quad (2)$$

where $s^a_{b'b} = s^a_{bb'} = 1$ when a, b and b' are different, and 0 otherwise; $|\text{vac}\rangle$ is the vacuum ($N_d = 0$) state. These states are labeled by the number of an unoccupied vertex.

We will fix $\epsilon_d = \frac{3}{2} U$ and consider the strong-coupling regime $v \ll \epsilon_d, U, J_H$ when N_d-fluctuations on each triangle are virtual and can be taken into account via a generalized Schrieffer-Wolff transformation $\mathcal{S}$ [21] (see also the Supplementary material, which contains Refs. [4, 5, 13, 21–33]) that includes processes shown in Fig. 1(b). A straightforward calculation yields the second-order KL Hamiltonian

$$H^{TTL}_{\rm ef} = \sum_{ka\sigma} \varepsilon_{k\sigma} c^\dagger_{ka\sigma} c_{ka\sigma} - \sum_{i\sigma ab} V_{ab} f^\dagger_{ia} f_{ib} c^\dagger_{ia\sigma} c_{ib\sigma} \quad (3)$$

that describes scattering of conduction electrons by the local VB singlets and is defined on a *non-frustrated* lattice whose sites correspond to triangles in Fig. 1(a). The coupling constants are $V_{ab} = V_\perp (1 - \delta_{ab}) + V_\parallel \delta_{ab}$ with $V_\perp = -\frac{v^2}{2\Delta}$, $V_\parallel = \frac{3v^2}{2\Delta}$, δ_{ab} – the Kronecker delta, and the valence fluctuation gap $\Delta = \frac{1}{2} U + \frac{3}{4} J_H$. The states (2) are described with a pseudo-fermion representation [5]:

$$|a\rangle_i \to f^\dagger_{ia} |\text{vac}\rangle \quad (4)$$

with a Hilbert space constraint $\sum_a f^\dagger_{ia} f_{ia} = 1$. Because only $S_d = 0$ triangle states are involved in the low-energy physics, interactions in $H^{TTL}_{\rm ef}$ preserve electron spin σ and only change the orbital (lead) degree of freedom a.

As a result, Eq. (3) describes a two-channel KL model (spin is the channel index) [34]. It is known that the two-channel fixed point is usually unstable w.r.t. channel asymmetry [34] controlled by the Zeeman splitting h. Since even for small $h \ll J_H$ the leads may be considered spin-polarized, below we omit the spin index σ and replace $c_{ia\sigma} \to c_{ia\uparrow} \equiv c_{ia}$ and $\varepsilon_{k\sigma} = \varepsilon_{k\uparrow} \approx \epsilon_k$.

The Hamiltonian (3) contains matrix elements connecting all three possible local VB states and conduction electron "flavors" a, and is an anisotropic (XXZ-like) $SU(3)$ KL model written in terms of generators $T^b_a(x_i) = f^\dagger_{ia} f_{ib}$ and $\tilde{\tau}^b_a(x_i) = c^\dagger_{ib} c_{ia}$ for local and itinerant degrees of freedom [35]. The local $SU(3)$ "spin"

operators $T^b_a(x_i)$ describe orbital fluctuations in Eq. (1) that flip the VB singlets (2). $H^{TTL}_{\rm ef}$ in Eq. (3) is invariant under $U(1)$ transformations $f_{ia} \to {\rm e}^{{\rm i}\phi_a} f_{ia}$ and $c_{ia} \to {\rm e}^{-{\rm i}\phi_a} c_{ia}$ that preserve the $V_\perp$ term. There is also a discrete lattice symmetry $C_{3v} = \{C_3, \sigma_v\}$ [23] that contains $\frac{2\pi}{3}$ (C_3) rotations around the TTL axis and three symmetry planes σ_v of the triangles.

Kondo effect-assisted VB phases. To demonstrate that the model (3) has a Kondo screened GS, we use a generalized hybridization mean-field (HMF) approach [36] that treats the f-fermion Hilbert space constraint on average, $\frac{1}{N}\sum_{ia}\langle f^\dagger_{ia} f_{ia}\rangle = 1$ (N is the system size), and self-consistently compute the hybridization and $SU(3)$ "magnetization" order parameters (OPs) [37]. We assume that all OPs are site-independent. There are three hybridization amplitudes: $\chi_0 = \frac{1}{\sqrt{3}}\sum_a \langle f_{ia} c_{ia}\rangle$, $\chi_{1,2} = \frac{1}{\sqrt{3}}\langle f_{i1}c_{i1} + \omega^{\mp 1} f_{i2} c_{i2} + \omega^{\pm 1} f_{i3} c_{i3}\rangle$ with $\omega = {\rm e}^{2\pi {\rm i}/3}$, and eight magnetizations m^c_l [m^f_l] for c- [f-] fermions defined via $\langle c^\dagger_{ia} c_{ib}\rangle = \sum_l \lambda^l_{ab} m^c_l + \frac{n^c}{3}\delta_{ab}$ [$\langle f^\dagger_{ia} f_{ib}\rangle = \sum_l \lambda^l_{ab} m^f_l + \frac{1}{3}\delta_{ab}$] where λ^l are the Gell-Mann matrices, $l = 1 \ldots 8$ and n^c is the conduction band filling. Unlike the real $SU(2)$ magnetization, $m^{c,f}$ do not break time-reversal invariance but rather the above $U(1)$ and C_{3v} symmetries. The OPs χ_1 and χ_2 are connected (up to a phase) by the planes σ_v from C_{3v}. Finite $m^{c,f}_{3,8}$ completely break C_{3v} leading to nematic states; $m^{c,f}_l$ with $l \neq 3, 8$ also break the above $U(1)$ symmetry. Kondo-screened states correspond to either OP $\chi_{0,1,2} \neq 0$. We call phases with $\chi_1 \neq \chi_2$ chiral, see the table in Fig. 2.

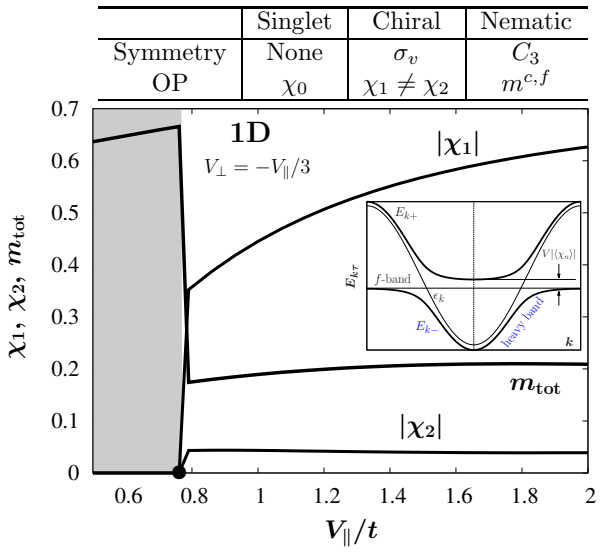

FIG. 2. $T = 0$ phase diagram of the KL model (3) with $N = 4900$ sites and electron density $n^c = 0.8$. $m_{\rm tot} = [(m^c_3 + m^f_3)^2 + (m^c_8 + m^f_8)^2]^{1/2}$ plays a role of the total magnetization. The black circle at $V_\parallel/t \sim 0.76$ marks the first order transition between Kondo-screened and normal phases. Inset: The HF band-structure. The band splitting at the Fermi level is $\sim V\chi_{1,2}$. The table shows symmetries broken by different OPs and corresponding VB liquid phases.

The phase diagram of the Hamiltonian (3) is shown in Fig. 2 for $\epsilon_k = -2t\cos k$ (t is the NN hopping). There is a first order transition between a normal state with $\chi_{0,1,2} = 0$, and a Kondo screened phase with $\chi_1 \neq \chi_2 \neq 0$ (but $\chi_0 = 0$) and non-zero $m^{c,f}_{3,8}$. This chiral nematic phase has delocalized VB singlets. The OPs $m^{c,f}$ survive only at low temperature $T \leqslant T_c \sim 5 \times 10^{-2} t$; for $T > T_c$ the only finite OP is χ_1 and the GS realizes a chiral metallic VB spin liquid.

Stability of the Kondo-assisted VB liquid. The Kondo phase in Fig. 2 is quite robust against changes in the noninteracting itinerant density of states (DOS). To show this, we consider a model DOS that corresponds to a square lattice with $\epsilon_k = -2t(\cos k_x + \cos k_y)$, see inset in Fig. 3. The phase diagram obtained by applying the HMF approach to the KL (3) is presented in Fig. 3. Unlike the 1D case in Fig. 2, the chiral VB liquid with $\chi_1 \neq 0$, $\chi_{0,2} = 0$ and $m^c = m^f = 0$ exists even at $T = 0$ for $V_\perp \leqslant 0$ and large $V_\parallel$. Only mirror symmetry from C_{3v} is broken by this state. With decreasing $|V_\perp|$ and $V_\parallel$ the system undergoes a transition to a nematic metallic state with $m^{c,f} \neq 0$ and completely broken C_{3v}. The situation is different for $V_\perp \geqslant 0$. Here the only non-zero OP is χ_0 and the VB liquid GS does not break any discrete symmetry. All these Kondo-screened states become unstable at small $|V_\perp|$ and $V_\parallel$.

The phase transitions in Fig. 2 and 3 are first order which may be an artifact of the HMF approximation. In general at $T = 0$ the emergence of nonzero OPs $\chi_{0,1,2}$ is associated with a *phase transition* (as opposed to a crossover) when fluctuations beyond HMF are taken into account [38]. Therefore salient features of our phase diagrams should remain unchanged.

Finally, we mention effects of a finite lead-mixing $H_{\rm mix}$ in Eq. (1). Its simplest form (compatible with C_{3v} symmetry of the TTL) corresponds to hopping of itinerant and local fermions around the triangle. This correction results [39] in a Zeeman-like term, proportional to the intra-triangle hopping, which lifts degeneracy of the local VB states (2) and can suppress the Kondo phase in Fig. 2 if this splitting is sufficiently large [4].

Implementation with ultracold AEAs. We propose an experimentally accessible implementation of the KL model (3) with AEAs in an optical lattice, *that is free of the mixing* described by $H_{\rm mix}$. The key idea of our approach is to use nuclear spin states of the atoms as "synthetic" frustrated plaquettes [corresponding to triangles in Fig. 1(a)] and construct an appropriate low-energy model that takes into account these local states as well as the itinerant degrees of freedom, and is unitarily related to the KL model (3). The GS degeneracy of a synthetic plaquette is guaranteed by the $SU(N = 3)$

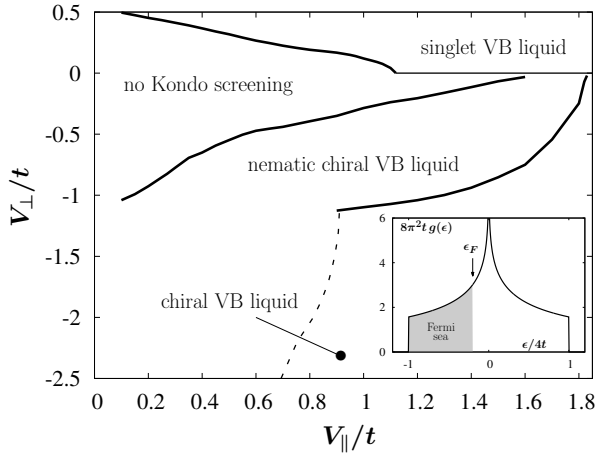

FIG. 3. Generic $T = 0$ phase diagram of Eq. (3) [or (7) with $U_{gg} = 0$] with $N = 3600$ sites and $n^c = 0.8$. All phase transitions are first order. Inside the nematic phase there is a "metamagnetic" transition between states with $m_1^{c,f} \neq 0$, $m_{3,8}^{c,f} = 0$ (at smaller $V_\parallel$) and $m_1^{c,f} = 0$, $m_{3,8}^{c,f} \neq 0$ (for larger $V_\parallel$) which are separated by a continuation of the dashed line. Inset: Noninteracting itinerant DOS $g(\epsilon) = \frac{1}{8\pi^2 t} K\big(\sqrt{1-(\epsilon/4t)^2}\big)$ [$K(x)$ is elliptic integral of the 1st kind] used to compute the phase diagram.

symmetry of the AEAs.

Consider a two-band optical lattice schematically shown in Fig. 1(d). The lowest-energy band is localized and contains two AEAs per site in different clock states: one ${}^1S_0$ (GS, g) and one ${}^3P_0$ (excited state, e). To minimize lossy e-e collisions, the higher-energy itinerant band is populated only by g atoms. The Hamiltonian of the system is [15]:

$$H^A = -t\sum_{\langle ij\rangle}(c_{in}^\dagger c_{jn} + \text{h.c.}) + \sum_i \Big[\frac{U_{gg}}{2} n_i^c(n_i^c - 1) + \quad (5)$$
$$+ \big(V_{gg} g_{in}^\dagger g_{im} + V'_{eg} e_{in}^\dagger e_{im}\big) c_{im}^\dagger c_{in} + V_{eg} e_{in}^\dagger e_{im} g_{im}^\dagger g_{in}\Big],$$

where g_{in} (e_{in}) denote g (e) fermions in the localized band at site i and nuclear spin state $n = \bar{1}$, 0, 1 [$\bar{n} = -n$, i.e. $\bar{1} = -1$, $\bar{0} = 0$], and $c_{in}^\dagger$ create itinerant g atoms. There is an implicit summation over nuclear spin indices. The first term describes nearest-neighbor hopping with an amplitude t. The second sum corresponds to e-g (V_{eg} and V'_{eg}) and g-g (V_{gg}) exchange couplings, as well as direct g-g interaction $U_{gg} \geqslant 0$ [see Fig. 1(d)-(f)]. V_{eg} and V'_{eg} have the same sign, and V_{gg} is negative [40].

States of a localized e-g pair are described by the term $H_{\rm loc}(x_i) = V_{eg} g_{in}^\dagger g_{im} e_{im}^\dagger e_{in}$ whose spectrum consists of a triply-degenerate GS subspace with energy $-V_{eg}$:

$$|l\rangle_i = \tfrac{1}{\sqrt{2}} \varepsilon_{lnm} e_{in}^\dagger g_{im}^\dagger |\text{vac}\rangle \quad (6)$$

(ε_{lnm} is the antisymmetric Levi-Civita tensor, $\varepsilon_{10\bar{1}} = 1$), and a sextet $|l\rangle_i' = (1/\sqrt{2}) s_{nm}^l e_{in}^\dagger g_{im}^\dagger |\text{vac}\rangle$ [s_{bc}^a was defined in (2)] and $|l\rangle_i'' = e_{il}^\dagger g_{il}^\dagger |\text{vac}\rangle$ with energy $+V_{eg}$. We assume that V_{eg} is large, $V_{eg} \gg |V_{gg}|, V'_{eg}, t$ [41], neglect mixing of the above sectors, and project the Hamiltonian (5) onto the subspace (6). Using the relations ${}_i\langle l|e_{in}^\dagger e_{im}|p\rangle_i = {}_i\langle l|g_{in}^\dagger g_{im}|p\rangle_i = \frac{1}{2}(\delta_{lp}\delta_{nm} - \delta_{ml}\delta_{np})$, and the pseudo-fermions (4), we obtain an effective model

$$H_{\rm ef}^A = \sum_{kl} \epsilon_k c_{kl}^\dagger c_{kl} - \sum_i \Big[V f_{il}^\dagger f_{ip} c_{il}^\dagger c_{ip} - \frac{U_{gg}}{2} n_i^c (n_i^c - 1)\Big] \quad (7)$$

with $V = \frac{V'_{eg} + V_{gg}}{2}$. If the states (6) are identified with VB singlets (2) on a triangle [Fig. 1(e)] by assigning a nuclear spin flavor m to each vertex, $H_{\rm ef}^A$ in 1D is equivalent to (spin-polarized) $H_{\rm ef}^{TTL}$ in Eq. (3) with $V_\perp = V_\parallel = V$ [42] plus a Hubbard term, whose role as well as possible ways to introduce anisotropic couplings in Eq. (7) we discuss below. To reach a Kondo screened GS one must have $V > 0$, i.e. $V'_{eg} > -V_{gg} > 0$ [43].

Discussion. In the presence of *extreme strong frustration* when only local spin *singlets* participate in the low-energy physics, the orbital fluctuations allow the conduction electrons to dynamically flip the VB singlets [see Fig. 1(b)], and stabilize a Kondo-screened phase with HF quasiparticles. We illustrated this mechanism within a periodic Anderson model on a frustrated TTL, and proposed an optical lattice setup that realizes this model with $SU(3)$-symmetric AEAs by using their nuclear spins to implement frustrated plaquettes (e.g. triangles).

Compared to the electronic KL (3), the low-energy model for AEAs (7) has several peculiarities. First, there is the Hubbard term U_{gg} which below half-filling enhances phases with non-zero $SU(3)$ magnetization in Fig. 3(b). However, its magnitude is effectively damped by the density prefactor $\sim (n^c)^2$. We checked that even when $n^c = 0.8$, one needs $U_{gg} > V$ to suppress the Kondo-screened state. Hence this term is unimportant for the Kondo physics. Second, the Hamiltonian $H_{\rm ef}^A$ has full $SU(3)$ symmetry (i.e. $V_\perp = V_\parallel$) that originates from the symmetry of Eq. (5) and prohibits experimental exploration of the phase diagram in Fig. 3. This symmetry can be broken by a weak external magnetic field B which to the lowest order amounts to replacing $V_\perp \to V_\perp + \frac{V_{gg} - V'_{eg}}{V_{eg}}(\mu_e - \mu_g)B$ ($\mu_{e,g}$ are magnetic moments for e and g atoms). Also, one might use other implementations of the $SU(3)$ Kondo effect [44], instead of our AEAs setup.

The HF phase in Figs. 2 and 3 can be detected in cold-atom experiments using slow quantum dynamics or time-of-flight measurements [45–47]. The KL model (7) can be implemented beyond 1D, which enables us to use AEAs as controlled [because of the $SU(N)$ symmetry] quantum simulators for more complex frustrated Kondo lattices. Although the currently available isotopes ^{87}Sr and ^{173}Yb are believed to have negative exchange couplings V [16–18], we expect that our results in Figs. 2 and 3 can be

realized with other AEAs.

Acknowledgments. We are grateful to Gia-Wei Chern and Michael Hermele for illuminating discussions. This work was supported by the NSF (PIF-1211914 and PFC-1125844), AFOSR, AFOSR-MURI, NIST and ARO individual investigator awards.

[1] H. Diep, *Frustrated Spin Systems* (World Scientific Publishing Company, Incorporated, 2004).
[2] C. Lacroix, P. Mendels, and F. Mila, *Introduction to Frustrated Magnetism: Materials, Experiments, Theory*, Springer Series in Solid-State Sciences (Springer Berlin Heidelberg, 2011).
[3] H.-Y. Kee and S. Julian, Physics in Canada **68**, 95 (2012).
[4] A. C. Hewson, *The Kondo Problem to Heavy Fermions* (Cambridge University Press, 1997).
[5] P. Coleman, Handbook of Magnetism and Advanced Magnetic Materials, Vol. 1, H. Kronmuller and S. Parkin (eds.) (2007).
[6] M. S. Kim and M. C. Aronson, Phys. Rev. Lett. **110**, 017201 (2013).
[7] P. Coleman and A. Nevidomskyy, Journal of Low Temperature Physics **161**, 182 (2010).
[8] Q. Si and S. Paschen, Physica status solidi (b) **250**, 425 (2013).
[9] J. H. Pixley, R. Yu, and Q. Si, Phys. Rev. Lett. **113**, 176402 (2014).
[10] B. H. Bernhard, B. Coqblin, and C. Lacroix, Phys. Rev. B **83**, 214427 (2011).
[11] J. Custers, K.-A. Lorenzer, M. Mller, A. Prokofiev, A. Sidorenko, H. Winkler, A. M. Strydom, Y. Shimura, T. Sakakibara, R. Yu, Q. Si, and S. Paschen, Nat. Mater. **11**, 189.
[12] M. N. Kiselev, International Journal of Modern Physics B **20**, 381 (2006).
[13] L. Isaev, K. Aoyama, I. Paul, and I. Vekhter, Phys. Rev. Lett. **111**, 157202 (2013).
[14] P. W. Anderson, in *Frontiers and borderlines in many-particle physics*, edited by R. Broglia and J. Schrieffer (North-Holland, Amsterdam, 1988).
[15] A. V. Gorshkov, M. Hermele, V. Gurarie, C. Xu, P. S. Julienne, J. Ye, P. Zoller, E. Demler, M. D. Lukin, and A. M. Rey, Nat. Phys. **6**, 289 (2010).
[16] X. Zhang, M. Bishof, S. L. Bromley, C. V. Kraus, M. S. Safronova, P. Zoller, A. M. Rey, and J. Ye, Science **345**, 1467 (2014).
[17] G. Cappellini, M. Mancini, G. Pagano, P. Lombardi, L. Livi, M. Siciliani de Cumis, P. Cancio, M. Pizzocaro, D. Calonico, F. Levi, C. Sias, J. Catani, M. Inguscio, and L. Fallani, Phys. Rev. Lett. **113**, 120402 (2014).
[18] F. Scazza, C. Hofrichter, M. Höfer, P. C. De Groot, I. Bloch, and S. Folling, Nat. Phys. **10**, 779.
[19] H. Katori, M. Takamoto, V. G. Pal'chikov, and V. D. Ovsiannikov, Phys. Rev. Lett. **91**, 173005 (2003).
[20] L. Balents, Nature **464**, 199 (2010).
[21] B. Mühlschlegel, Zeitschrift für Physik **208**, 94 (1968).
[22] C. D. Batista and G. Ortiz, Advances in Physics **53**, 1 (2004).
[23] G. Bir and G. Pikus, *Symmetry and Strain-Induced Effects in Semiconductors* (John Wiley and Sons, 1974).
[24] J. Blaizot and G. Ripka, *Quantum Theory of Finite Systems* (Cambridge, MA, 1986).
[25] P. Coleman and N. Andrei, Journal of Physics: Condensed Matter **1**, 4057 (1989).
[26] K. Ingersent, A. W. W. Ludwig, and I. Affleck, Phys. Rev. Lett. **95**, 257204 (2005).
[27] T. Kuzmenko, K. Kikoin, and Y. Avishai, Phys. Rev. Lett. **96**, 046601 (2006).
[28] R. López, T. c. v. Rejec, J. Martinek, and R. Žitko, Phys. Rev. B **87**, 035135 (2013).
[29] A. K. Mitchell, T. F. Jarrold, M. R. Galpin, and D. E. Logan, The Journal of Physical Chemistry B **117**, 12777 (2013), pMID: 23527540.
[30] K. Okunishi, M. Sato, T. Sakai, K. Okamoto, and C. Itoi, Phys. Rev. B **85**, 054416 (2012).
[31] D. S. Saraga and D. Loss, Phys. Rev. Lett. **90**, 166803 (2003).
[32] K. Seki and K. Okunishi, Phys. Rev. B **91**, 224403 (2015).
[33] V. Zaitsev and A. Polyanin, *Handbook of Exact Solutions for Ordinary Differential Equations* (CRC Press, 2002).
[34] D. L. Cox and A. Zawadowski, *Exotic Kondo Effects in Metals: Magnetic Ions in a Crystalline Electric Field and Tunnelling Centres* (Taylor & Francis, 1999).
[35] A. Auerbach, *Interacting Electrons and Quantum Magnetism*, Graduate Texts in Contemporary Physics (Springer New York, 1994).
[36] S. Viola Kusminskiy, K. S. D. Beach, A. H. Castro Neto, and D. K. Campbell, Phys. Rev. B **77**, 094419 (2008).
[37] See the Supplementary material.
[38] T. Senthil, M. Vojta, and S. Sachdev, Phys. Rev. B **69**, 035111 (2004).
[39] See the Supplementary material.
[40] Because the s-wave scattering length is $a_{gg} > 0$ [15], two-atom collisions favor antisymmetric spatial wavefunction and symmetric nuclear spin configurations.
[41] V_{eg} is at least twice larger than V'_{eg} and $|V_{gg}|$ because of the Bloch-function overlap between lowest and excited bands. This overlap can be further decreased by placing itinerant g atoms in higher bands.
[42] The C_{3v} operations should be applied to nuclear spin states: C_3 performs a cyclic permutation $10\bar{1} \to \bar{1}10$, and σ_v's interchange any two states while preserving the third, e.g. $10\bar{1} \to \bar{1}01$.
[43] See the renormalization group analysis in the Supplementary Material.
[44] Y. Nishida, Phys. Rev. Lett. **111**, 135301 (2013).
[45] M. Foss-Feig, M. Hermele, and A. M. Rey, Phys. Rev. A **81**, 051603 (2010).
[46] M. Foss-Feig, M. Hermele, V. Gurarie, and A. M. Rey, Phys. Rev. A **82**, 053624 (2010).
[47] B. Paredes, C. Tejedor, and J. I. Cirac, Phys. Rev. A **71**, 063608 (2005).